Available online at www.sciencedirect.com
SCIENCE DIRECT®
Polymer 45 (2004) 961–971
polymer
www.elsevier.com/locate/polymer

# Miscible blends of syndiotactic polystyrene and atactic polystyrene. Part 1. Lamellar morphologies and diluent segregation

Chi Wang[a,*], Wei-Po Liao[a], Yong-Wen Cheng[a], Tsang-Lang Lin[b]

[a]Department of Chemical Engineering, National Cheng Kung University, 1, University Road, Tainan 701, Taiwan, ROC
[b]Department of Engineering and System Science, National Tsing Hua University, Hsin-Chu 300, Taiwan, ROC

Received 9 August 2003; received in revised form 20 November 2003; accepted 4 December 2003

**Abstract**

Lamellar morphologies of melt-crystallized blends of syndiotactic polystyrene (sPS, weight-average molecular weight $M_w = 200$ k) and atactic polystyrene (aPS, $M_w = 100$k) have been investigated using small-angle X-ray scattering (SAXS) and transmission electron microscopy (TEM). sPS/aPS blends with various compositions were prepared and crystallized isothermally at 250 °C prior to morphological studies. Due to the proximity in the densities of the crystal and amorphous phases, a weak SAXS reflection associated with lamellar microstructure was obtained at room temperature. In addition, strong diffuse scattering at low scattering vectors was evidently observed and its appearance may obscure the intensity maximum associated with the lamellar features, leading to the difficulties in determining the microstructure of the blends. To enhance the density contrast, SAXS intensities at an elevated temperature of 150 °C were measured as well to deduce the morphological results with better precision. Based on the Debye–Bueche theory, the intensities of the diffuse scattering were estimated and subtracted from the observed intensities to obtain the scattering contribution exclusively from the lamellar microstructure. Morphological parameters of the sPS/aPS blends were derived from the one-dimensional correlation function. On addition of aPS, no significant changes in the lamellar thickness have been found and the derived lamellar thicknesses are in good agreement with TEM measurements. Segregation of rejected aPS components during sPS crystallization was evidently observed from TEM images which showed aPS pockets located between sPS lamellar stacks and distributed uniformly in the bulk samples, leading to the interfibrillar segregation.


*Keywords:* Lamellar morphology; Diluent segregation; Syndiotactic polystyrene

## 1. Introduction

Compared to its isomers, the recently-developed syndiotactic polystyrene (sPS) show much promise as an engineering thermoplastics due to its high melting temperature and low dielectric constants. The widespread interest in this stereo-regular and crystallizable material has motivated many investigations on its conformation, configuration, crystal structure and crystallization kinetics to compensate the knowledge gap between its isotactic and atactic counterparts (iPS and aPS) which have been extensively studied in the past several decades. Although a considerable amount of research has been conducted on sPS in the last decade [1–10], systematic lamellar morphology of neat sPS and its related blends are seldom reported, as far as the authors are aware.

Improved polymer properties through blending with others continue to be an area of active industrial as well as academic concerns and ones of much intensive research effort. Miscibility of sPS and aPS in the melt state has been already demonstrated by several researchers [11–14]. For sPS/aPS blends, it has been pointed out that the addition of aPS results in the retardation of sPS crystallization [14,15]. Thus far, however, there have been no studies that specifically address the effects of aPS addition on the microstructures of sPS/aPS blends. It has been known that the introduction of amorphous diluent to crystallizable polymer chains is likely to change the morphology of mother polymers, leading to a drastic variation of apparent properties. Of particular interest is the location of the added diluent. Depending on the segregation level of the amorphous/crystalline pair, three categories can be

* Corresponding author. Tel.: +886-62378422; fax: +886-62344496.
*E-mail address:* chiwang@mail.ncku.edu.tw (C. Wang).

0032-3861/$ - see front matter © 2003 Elsevier Ltd. All rights reserved.
doi:10.1016/j.polymer.2003.12.009

classified, i.e. interlamellar, interfibrillar and interspherulitic placement of the amorphous diluents, when the crystallizable component is crystallized from the miscible state [16,17]. Considerable effort in understanding the placement of the added diluents should center on an understanding of the microstructure change after blending. Significant contributions to this understanding can be provided by transmission electron microscopy (TEM) and small-angle X-ray scattering (SAXS) techniques. In the present paper we concentrate on the lamellar morphology of sPS, particularly in the influence of the aPS content. A subsequent report will discuss the crystal growth of sPS/aPS blends and the surface free energies of sPS lamelle in the presence of aPS diluents.

## 2. Experimental

### 2.1. Materials

The sPS pellets with a weight-average molecular weight ($M_w$) of 200 kg/mol were obtained from Dow Chemical Co. The aPS samples were purchased from Aldrich Co. with $M_w = 100$ kg/mol and a polydispersity index of 2.1. The glass transition temperature and transition breadth of aPS are 100.0 and 5.7 °C, respectively.

### 2.2. Blend preparation

Various ratios of sPS/aPS blends were prepared by dissolving the calculated amount of individual components in *ortho*-dichlorobenzene (*o*-DCB) solvent at 140 °C to produce 1% (w/v) solutions. After 2 h thermal equilibrium in the oil bath, the homogeneous solution was then precipitated into a 20-fold excess volume of methanol. The precipitated sPS/aPS powders were thoroughly washed with fresh methanol to remove residual *o*-DCB. Final drying of the precipitated polymer blend was accomplished by maintaining the samples under vacuum. In this manner, sPS/aPS blends with verified compositions from 90/10 to 10/90 in weight-percent ratio were prepared, the first number denoting sPS component throughout this paper.

To prepare the sPS/aPS blends for morphological studies, the collected blend flakes were melt-pressed in a small disk-shaped mold with a diameter of 6.5 mm and thickness of 1.5 mm at 290 °C and 0.6 MPa for 10 min, followed by the ambient cooling at atmosphere pressure. The small sPS disks were enclosed in DSC aluminum pans and thermal equilibrated at 300 °C in a Mettler hot stage (FP-82) for 10 min. Then, the samples were quickly shifted to another well-controlled hot stage (THMS600, Linkam) for isothermal crystallization at 250 °C for 2 h. Crystallization was ceased by quenching the samples to liquid nitrogen.

### 2.3. WAXD measurements

To characterize the crystal form of the sPS/aPS blends, wide-angle X-ray diffraction (WAXD) patterns of the crystallized samples were obtained using a RINT2000 X-ray goniometer (Rigaku, Cu target) operated at 40 kV and 30 mA with a $2\theta$ scan speed of 1°/min and sampling width of 0.05°. WAXD pattern of completely amorphous sPS was also obtained from a sample, which has been melted at 300 °C and then quenched in liquid nitrogen.

### 2.4. SAXS measurements

SAXS profiles of these samples were obtained at room temperature using a 18kW rotating anode X-ray generator (Rigaku, Cu target) operated at 40 kV and 100 mA. A set of three pinholes collimators was used. A $20 \times 20$ cm$^2$ position-sensitive area detector (ORDELA Model 2201X, Oak Ridge Detector Laboratory Inc.) with $256 \times 256$ channels was used to collect the SAXS data. For the performance of SAXS measurements at high temperatures, a heating device, consisting of a flexible electric-heating belt to wrap the sample assembly, and a well-performed feedback system for temperature control were used to thermally equilibrate the sPS samples. The temperature was kept constant, with variations of less than $\pm 0.5$ °C, and the SAXS intensities were accumulated for an appropriate period of time to attain a sufficient S/N ratio. The SAXS patterns were corrected for blank scattering, sample thickness and adsorption. The area scattering intensities were averaged azimuthally to obtain the one-dimensional (1-D) intensity profile for further analyses. The scattering vector is defined as $q = 4\pi \sin\theta/\lambda$, where $2\theta$ is the scattering angle and $\lambda$ is the wavelength of X-ray. The sample to distance was about 4000 mm, covering a scattering vector $q$ from 0.11 to 3.0 nm$^{-1}$. By means of a pre-calibrated secondary standard (slightly cross-linked polyethylene sample), the data were converted to an absolute differential cross-section with a unit of cm$^{-1}$. Details of SAXS setup was described elsewhere [18,19]. Corrections for thermal density fluctuations were carried out with the aid of the Porod law given as follows,

$$\lim_{q\to\infty} [K_p - (I_{obs} - I_{fl})q^4 \exp(\sigma^2 q^2)] = 0 \quad (1)$$

where $I_{fl}$ arises from thermal density fluctuations, $K_p$ is the Porod constant and $\sigma$ is the interfacial thickness between the crystalline and amorphous regions. After the optimal parameters ($I_{fl}$, $K_p$ and $\sigma$) are determined numerically, the corrected intensities $I_{cor} = (I_{obs} - I_{fl})\exp(\sigma^2 q^2)$ are used for further analyses.

### 2.5. TEM observation

The thin sections, ca. 50 nm thick, to be observed by TEM were prepared by cutting the samples at room temperature using an Ultracut UCT (Leica) microtome. Staining of the thin sections was subsequently carried out at room temperature with ruthenium tetraoxide ($RuO_4$) vapors.

The TEM micrographs shown in this work were done with a JEM-2000FX (Jeol) microscope operated at 80 kV.

### 2.6. DSC measurements

Melting behavior of sPS/aPS blends was measured using a Perkin–Elmer DSC7 from 23 to 300 °C with a heating rate of 10 °C/min under nitrogen atmosphere to diminish oxidation. Indium and zinc standards were used to calibrate the enthalpies of fusion and melting temperatures prior to DSC experiments. The glass transition temperatures ($T_g$) were taken as the midpoint of the heat capacity changes. The melting temperature was reported at the peak of the melting endotherm and the area of endotherm gave the melting enthalpy.

### 2.7. POM observation

Using a polarized optical microscope (POM, Leica DMLP) equipped with a hot stage (THMS600, Linkam), the spherulitic (and axilitic) morphology of the sPS/aPS blends was observed. sPS/aPS powders were melted at 300 °C for 10 min and then rapidly cooled to 250 °C for isothermal crystallization. Sizes of the spherulites were measured through a recording system. Crystal growth rates ($G$) were determined from the slope of spherulitic radius versus elapsed time. Linear growth of spherulites was observed for all the blends investigated in this study.

## 3. Results and discussion

All sPS/aPS blends demonstrate the β′-form crystals (orthorhombic unit cell [1]) according to their WAXD patterns. Fig. 1 shows the typical WAXD diffractograms of the neat sPS and 50/50 blend. The indexed planes for each diffraction peaks agree well with the characteristic peaks of the disordered β′ polymorph, indicating the presence of β′-form after addition of aPS diluents in accordance with the previous report [13]. The intensity profile of completely amorphous sample is also shown in Fig. 1 as broken line in an attempt at determining the weight fraction of crystallinity ($\phi_w^{WAXD}$). It is superimposed on the WAXD profiles of crystallized sPS/aPS blends by scaling the intensities at 8, 15, 22.5 and 28°. The crystallinity fraction is then derived from the ratio of integrated intensities from all the crystalline peaks to the total intensity curve. On addition of aPS diluents, the amount of crystallizable sPS chains is reduced due to the dilution effect, giving a smaller $\phi_w^{WAXD}$ in the blends. Nevertheless, the normalized $\phi_w^{WAXD}$ with the weight fraction of sPS, i.e. $\phi_w^{WAXD}/(1 - w_{aPS})$, remains the same regardless of the aPS content in the blend.

Melting behavior of sPS/aPS blends was investigated using DSC heating traces. Two melting peaks are evidently observed for most blends except the 10/90 blend where a single melting peak is found. Double melting behavior

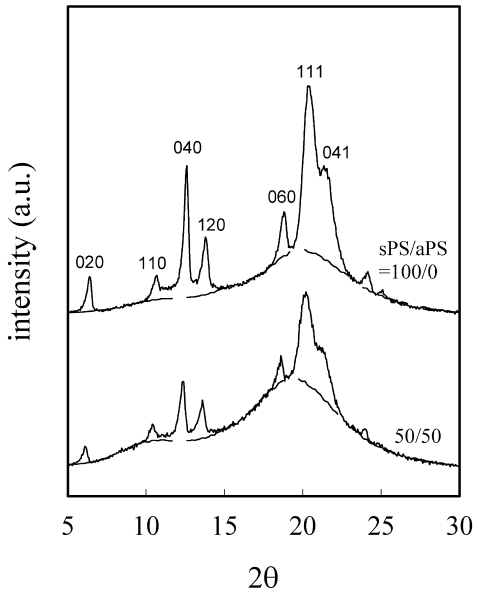


Fig. 1. WAXD profiles for sPS/aPS samples crystallized isothermally at 250 °C for 2 h (the broken lines are WAXD profiles of completely amorphous sPS superimposed on that for sPS by scaling the intensities at $2\theta = 8$, 15, 22.5 and 28°).

suggests the coexistence of two lamellar thicknesses (perfections) or/and the occurrence of melting-recrystallization—remelting phenomena during the DSC heating scan. The detailed investigation referred to the double melting behavior is in progress and will be discussed in future report. The melting temperatures are referred to $T_{ml}$ and $T_{mh}$ for the low and high temperatures, respectively. Both $T_{ml}$ and $T_{mh}$ are plotted in Fig. 2 versus blend composition. No significant changes of melting temperatures are observed with respect to neat sPS, being ca. 264 and 271 °C for $T_{ml}$ and $T_{mh}$. The single melting temperature of the 10/90 blend is close to the $T_{ml}$ of the other blends, indicating that the presence of thicker lamellae (or recrystallization behavior) is substantially depressed in blends having high aPS content. Basically, Fig. 2 shows that the melting behavior of sPS

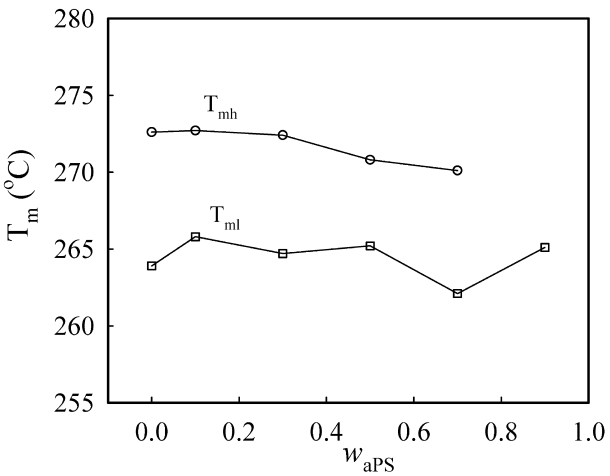


Fig. 2. Melting temperatures of sPS/aPS blends determined from DSC heating scans.

remains merely unaffected by the amount of aPS present in the blend, suggesting that the lamellar thickness is relatively independent of blend composition. After extracting the melting enthalpies from DSC thermograms, the crystallinity fractions of each blend ($\phi_w^{DSC}$) were also determined by assuming an enthalpy of fusion of 82.4 J/g for perfect sPS crystals [20]. A comparison of the weight fraction of crystallinity determined from DSC and WAXD is given in Fig. 3 from which quite good agreement is seen between the two data sets.

It is well known that the crystallization kinetics and morphology of polymers are strongly dependent on the amount of supercooling $\Delta T(= T_m^0 - T_c$, where $T_m^0$ and $T_c$ are the equilibrium melting temperature and crystallization temperature, respectively). Thus, it is desirable to determine the $T_m^0$ for each blend on the basis of linear Hoffman–Weeks plots as shown in Fig. 4 where the observed melting temperatures of blends isothermally-crystallized at various $T_c$ are plotted as a function of $T_c$. The lower melting point is used in Fig. 4 when double melting behavior, which is commonly observed for sPS/PS blends crystallized at low $T_c$, is detected. As shown in Fig. 4, the extrapolated $T_m^0$ values for neat sPS and sPS/aPS blends are approximately the same (ca. 291 °C) regardless of aPS content, indicating that the interaction parameter ($\chi$) between sPS and aPS is virtually zero which is quite reasonable in comparison with the similar pair of iPS/aPS blends ($\chi = -0.003$) [21]. Indeed, for all crystallized blends the variation of $T_m^0$ and $T_g$ is rather small as shown in Table 1; $T_g$ were measured from the DSC heating scan and $T_m^0$ were derived theoretically on the basis of the Flory–Huggins treatments [22] with $T_m^0$ of 291 °C for neat sPS [23,24]. Also given in Table 1 is the crystal growth rate of sPS at 250 °C measured by POM. The growth rate of sPS is substantially reduced with increasing aPS content due mainly to a dilution effect since the degree

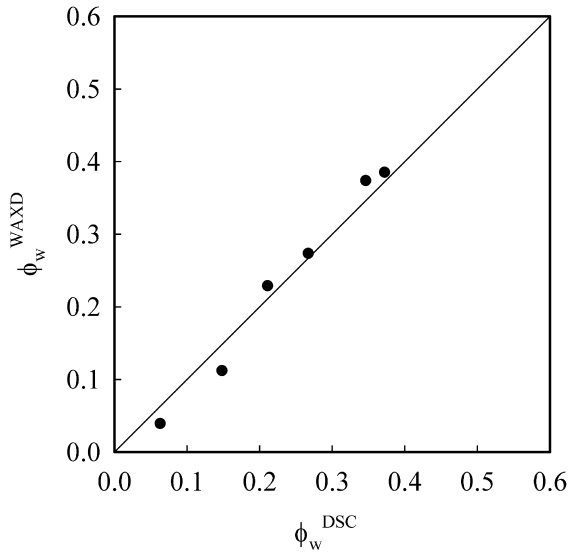


Fig. 3. A comparison of weight fraction of crystallinity, $\phi_w$, obtained from DSC and WAXD.

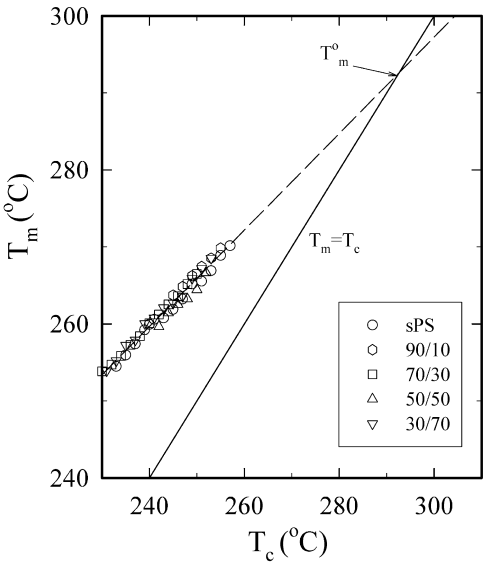


Fig. 4. Hoffman–Weeks plots for neat sPS and sPS/aPS blends crystallized isothermally at various temperatures.

of supercooling is the same for all blends. Moreover, the degree of growth rate depression is roughly in proportion to the amount of aPS added.

### 3.1. SAXS measurements

The Lorentz-corrected SAXS intensity profiles for samples measured at 25 °C are given in Fig. 5(a). To enhance the scattering contrast, SAXS at 150 °C has been also conducted and the results are plotted in Fig. 5(b). In order to facilitate better comparison, the plots are drawn to the same scales. At 25 °C, a distinct scattering maximum at $q = 0.3415\ nm^{-1}$ is detected for neat sPS, suggesting the presence of lamellar microstructures. On addition of aPS, the scattering peak is gradually diminished with increasing aPS content, indicating the reduction of lamellar population. The maxima shift slightly to lower $q$ values for blends containing up to 30 wt% aPS. For 50/50 and 30/70 blends, no discernible maximum but a scattering plateau is observed. When SAXS is conducted at 150 °C, a similar trend is observed but the scattering maximum becomes

Table 1
Glass transition temperature ($T_g$), equilibrium melting temperature ($T_m^0$) and crystal growth rate ($G$) for sPS/aPS blends

| sPS/aPS | $T_g$ (°C)[a] | $T_m^0$ (°C)[b] | $G$ (nm/s) |
|---|---|---|---|
| 100/0 | 97.8 | 291.0 | 98.1 |
| 90/10 | 96.0 | 291.0 | 87.2 |
| 70/30 | 97.7 | 290.9 | 74.8 |
| 50/50 | 99.9 | 290.8 | 50.0 |
| 30/70 | 97.8 | 290.7 | 39.5 |

[a] $T_g$ was determined from the heating scan (10 °C/min) of the isothermally crystallized blends.
[b] $T_m^0$ was obtained from the Flory–Huggins equation [22] using $T_m^0 =$ 291 °C for neat sPS [23].

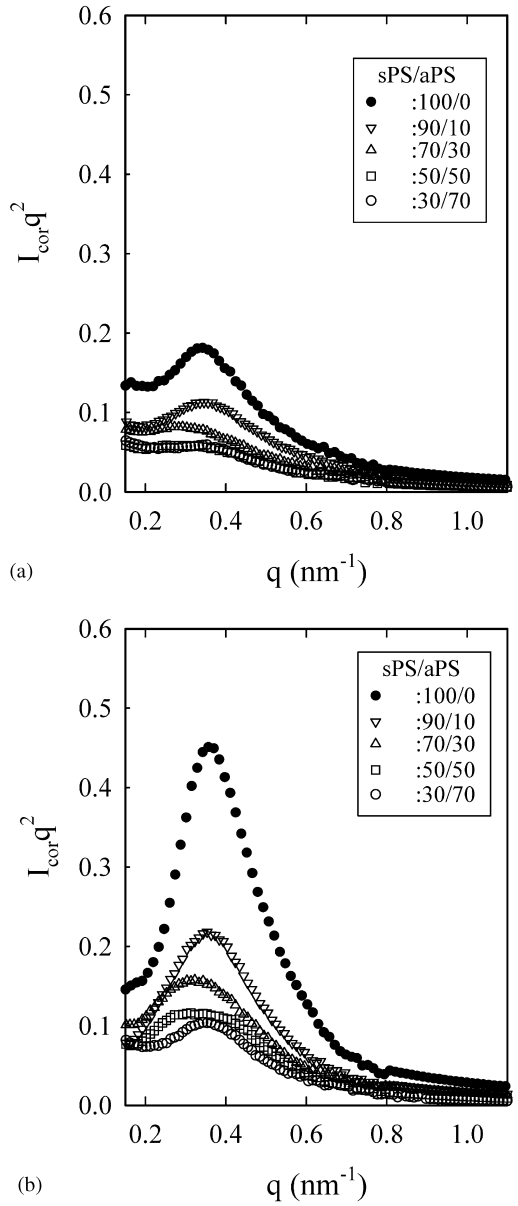


Fig. 5. Lorentz-corrected SAXS intensities as a function of scattering vector for sPS/aPS blends measured at (a) 25 °C, (b) 150 °C.

more distinct, providing a more precise determination of long period. For 50/50 and 30/70 blends, a small but discernible maximum can be detected as shown in Fig. 5(b). The position of the intensity maximum ($q_m$) was used to derive the long period $L_B(=2\pi/q_m)$ in accord with the Bragg's law. Table 2 lists the $L_B$ deduced for various blends. In addition to the scattering peak, it has to be noted that diffuse scattering appears near the beam stop, leading to an anomalous rise in intensity at low $q$ regions. The strong diffuse scattering may obscure the scattering associated with the lamellar microstructure and further make the determination of long period more difficult. It is especially evident for SAXS measurement at 25 °C for 50/50 and 30/70 blends. The intensity for the diffuse scattering is relatively independent of the test temperature but gradually reduced

Table 2
A comparison of long periods determined respectively from Lorentz-corrected intensity plots of SAXS measurements at 25, 150 °C and difference scattering

| sPS/aPS | $L_B$ (nm)[a] | | $L'_B$ (nm)[b] | | $L_B$ (nm) Difference scattering |
|---|---|---|---|---|---|
| | 25 °C | 150 °C | 25 °C | 150 °C | |
| 100/0 | 18.4 | 17.3 | 17.3 | 17.0 | 17.1 |
| 90/10 | 17.5 | 17.5 | 17.5 | 17.3 | NA |
| 70/30 | 21.6 | 19.4 | 19.4 | 17.8 | 18.3 |
| 50/50 | NA | 18.4 | NA | 17.3 | 17.5 |
| 30/70 | NA | 17.7 | NA | 17.3 | 17.1 |

[a] $L_B$ is the long period obtained from the original SAXS intensities (Fig. 5).
[b] $L'_B$ is the long period obtained from the SAXS intensities excluding the diffuse scattering effect (Fig. 8).

with increasing aPS content. The presence of diffuse scattering indicates the existence of another scattering mechanism different from the one associated with lamellar structure developed in the blends [19,24–29]. The authentic cause of the diffuse scattering has not been fully realized yet although several proposals have been offered, for example: the presence of microvoids, a grain boundary phase, single lamellae, isolated amorphous zone, and foreign particles. Previously, we have successfully applied the Debye–Bueche (DB) model to account for the diffuse scattering for neat sPS melt-crystallized at various temperatures [24]. It seems that diffuse scattering is a predominant feature for neat sPS as well as for its blends with aPS. The DB model describes the intensity ($I_o$) scattered by the random distribution of heterogeneity, as follows,

$$I_o = A/(1 + a_c^2 q^2)^2 \quad (2)$$

where $A$ is a constant related to the scattering contrast between the heterogeneous domains and the surrounding and $a_c$ is a correlation length which is relevant to the heterogeneous domains. On the basis of Eq. (2), a plot of $I^{-0.5}$ versus $q^2$ will give a straight line at low $q$ regions and $a_c$ value is obtained from the square root of slope/intercept ratio. Fig. 6 shows such a plot for sPS/aPS blends measured at 150 °C, and the derived $a_c$ values as a function of aPS content are given in Fig. 7. It is interesting to note that $a_c$ is increased gradually as more aPS is added in the blend, ca. 5.5 nm for neat sPS and 8.2 nm for 30/70 blends. Moreover, $a_c$ is slightly smaller at 150 °C than at 25 °C for all blends except the 90/10 blend where a more apparent variation is observed. After subtracting the diffuse scattering intensity from the observed scattering intensity to deduce the contribution exclusively from lamellar microstructure [19,24], the derived plots of $(I_{cor} - I_o)q^2$ versus $q$ are given in Fig. 8, where a more appropriate determination of the long period can be made. As the aPS content increases, the maximum of the scattering peak shifts slightly towards smaller $q$. The magnitude of scattering peak, however,

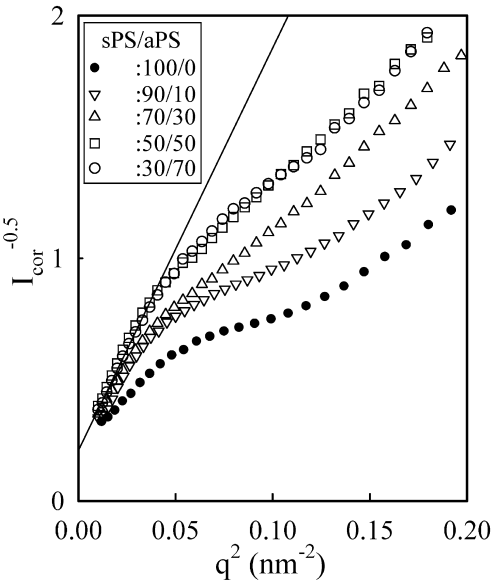


Fig. 6. Debye–Bueche plots of SAXS intensity data measured at 150 °C to determine the correlation length $a_c$ relevant to the diffuse scattering.

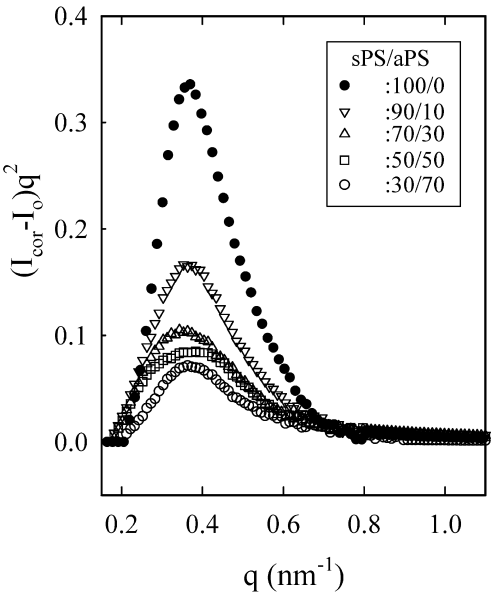


Fig. 8. Lorentz-corrected SAXS intensities as a function of scattering vector for sPS/aPS blends measured at 150 °C after subtraction of the contribution from the diffuse scattering.

decreases monotonically with increasing aPS content, which is typical of the dilution effect. It would be desirable to make a detailed comparison of long periods obtained from different approaches. Given in Table 2 is a comparison of long periods deduced from the Bragg's law with ($L_B'$) and without ($L_B$) taking the diffuse scattering into consideration. Also tabulated in Table 2 are the long periods obtained from a 'difference scattering approach' [29] where the intensities measured at 25 °C were subtracted from those measured at 150 °C to exclude the contribution from the diffuse scattering [19]. Fig. 9 shows the 'difference scattering' patterns for each blend and the long periods are derived from the scattering maxima. It is of interest to note the absence of the diffuse scattering at low $q$ region when 'difference scattering' approach is carried out for morphological analyses. As shown in Table 2, the long periods obtained from SAXS at 150 °C and from the 'difference scattering' approach agree with each other, suggesting the validity of DB model to describe the diffuse scattering. However, the long period derived from SAXS at 25 °C is relatively large. As shown in Fig. 5(a), the weak scattering peak associated with the lamellae may be masked and become barely seen by the presence of strong diffuse scattering. Indeed, measurement difficulties have been encountered in determining the accurate $q_m$ for 50/50 and 30/70 blends. It comes to a conclusion that SAXS at high

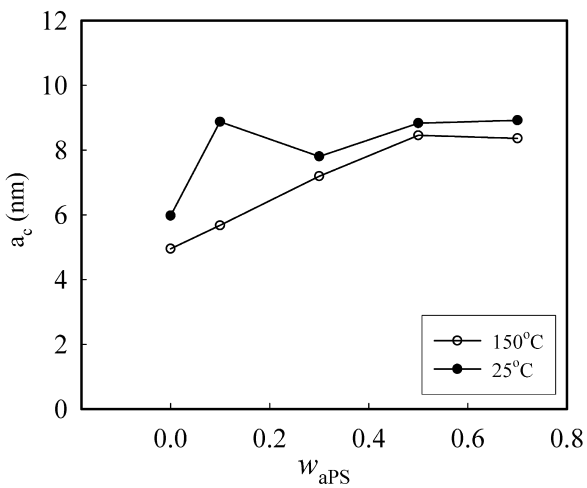


Fig. 7. Correlation length $a_c$ for the diffuse scattering as a function of aPS weight fraction.

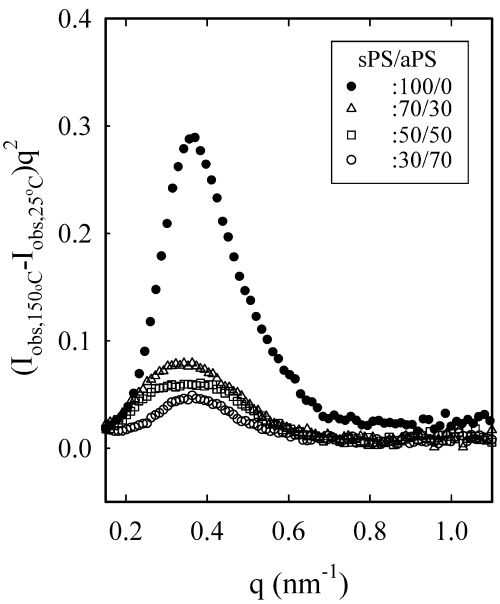


Fig. 9. Lorentz-corrected SAXS intensity profiles of sPS/aPS blends on the basis of 'difference scattering' method.

temperature (e.g. 150 °C) is more appropriate to deduce reliable microstructure results.

Based on the 1-D correlation function that describes the electron density variation along the lamellar normal, an analysis of SAXS data was further performed. After taking the Fourier transformation of the scattering intensity distribution $I(q) = I_{cor} - I_o$ exclusively resulting from the lamellar microstructure, the 1-D correlation function $\gamma(z)$ can be given by [30–32]

$$\gamma(z) = \int_0^\infty I(q)q^2 \cos(qz)\mathrm{d}q / \int_0^\infty I(q)q^2 \,\mathrm{d}q \tag{3}$$

The denominator denotes the scattering invariant ($Q$) that is related to the linear crystallinity $\phi_c^{lin}$, as follows [31,33]

$$Q = \phi_s \phi^{lin}(1 - \phi^{lin})(\Delta\rho)^2 \tag{4}$$

where $\phi_s$ is the volume fraction filled with the lamellar stacks and $\Delta\rho$ is the difference between the densities of the lamellar and amorphous regions. The linear crystallinity ($\phi^{lin}$) defined as the ratio of lamellar thickness to the long period both obtained from the correlation function is the crystallinity within the alternating crystalline/amorphous layer superstructure (or lamellar stacks). To reveal the effects of temperature and aPS contents on the observed SAXS intensities, the evaluation of scattering invariant $Q$ for each blend is performed from the integration of those curves in Fig. 8 and results are given in Fig. 10 as a function of aPS content. Addition of aPS reduces the scattering invariant and a larger $Q$ is found at 150 °C, compared with that at 25 °C. Based on the DSC thermographs of heating scans, no crystal melting is detected at 150 °C. Thus, the increase of $Q$ is attributed to the contrast enhancement of a larger value of $\Delta\rho$ since both $\phi_s$ and $\phi_c^{lin}$ remains intact according to Eq. (4).

Evaluation of the morphological parameters of the sample is based on the properties of the 'self-correlation triangle'. According to the previous work by Strobl et al. [30], the position of the first maximum denotes the long period ($L_c$). Simple relations between the thicknesses of the crystalline lamella ($l_c$) and amorphous layer ($l_a$) are given to deduce individual values; i.e. $l_c + l_a = L_c$ and $l_c l_a = L_c B$, where $B$ is the position of the first zero of the correlation function [30,31]. The derived values of $l_c$, $l_a$ and $L_c$ are collected in Fig. 11. It is evident that a consistent but smaller long period is obtained from the 1-D correlation function in comparison with that estimated by the Lorentz-corrected plots. It should be noted that there exists a distribution for the long period; its most probable value is obtained from the 1-D correlation function, whereas the Lorentz-corrected plot provides the mass-averaged result. The assignments of $l_c$ and $l_a$ are in good agreement with TEM micrograph (Fig. 13, discussed later), which shows the lamellar thickness distribution in a range of 5–9 nm. Up to 30 wt% aPS inclusions, as shown in Fig. 11, a modest increase of the long period is observed from 15.6 nm for neat sPS to 16.9 nm for 70/30, primarily due to an increase in amorphous layer thickness (from 9.3 to 11.5 nm, correspondingly). Further increasing incorporation of aPS would result in a reduction in $l_a$, which in turn leads to a reduction in long period. For all blends $l_c$ decreases only slightly with increasing aPS content, as shown in Fig. 11. This is consistent with the melting temperature measured by DSC (Fig. 2), where relatively constant $T_m$ can be seen for all the blends studied. The calculated values of $\phi^{lin}$ for various blends are given in Fig. 12. Also given in Fig. 12 is the derived $\phi_s$, determined from a simple relation by: $\phi_v = \phi_s \phi^{lin}$, where $\phi_v$ is the volume fraction of crystallinity [$= (\rho/\rho_c)\phi_w$, where $\rho$ and $\rho_c$ are the sample density and crystalline density, respectively]. Provided that both $\phi_v$ and $\phi^{lin}$ are known, the volume fraction occupied by the lamellar stacks is estimated by the value of the $\phi_v/\phi^{lin}$ ratio. If the sample is completely filled with the superstructure, the $\phi_v/\phi^{lin}$ ratio is 1.0. Otherwise, a smaller value

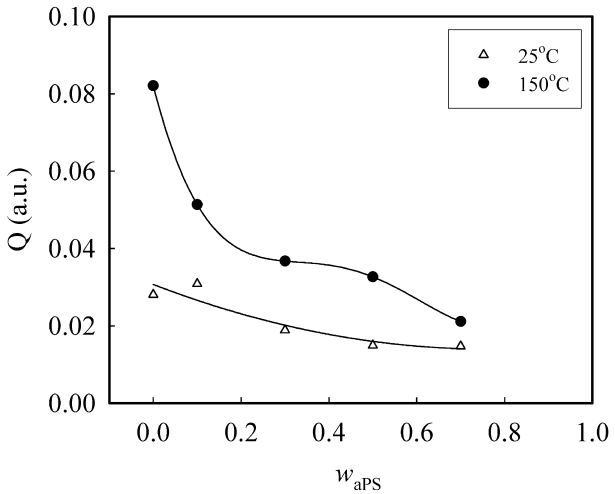


Fig. 10. Calculated scattering invariants, $Q$, for sPS/aPS blends measured at 25 and 150 °C.

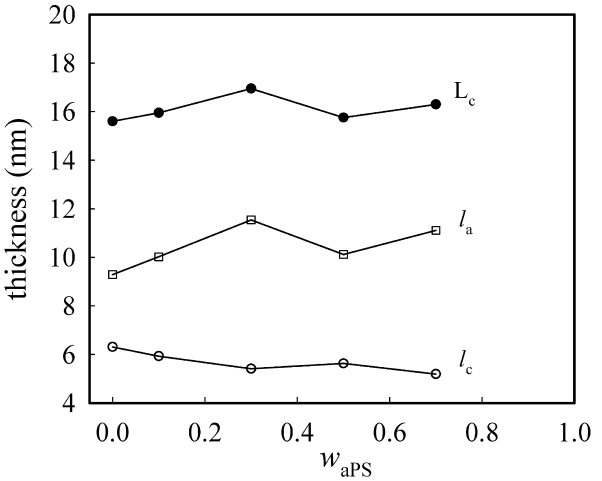


Fig. 11. Variation of long period $L_c$, lamellar thickness $l_c$ and amorphous layer thickness $l_a$ with aPS weight fraction; the morphological parameters are determined from 1-D correlation function of SAXS intensities measured at 150 °C.

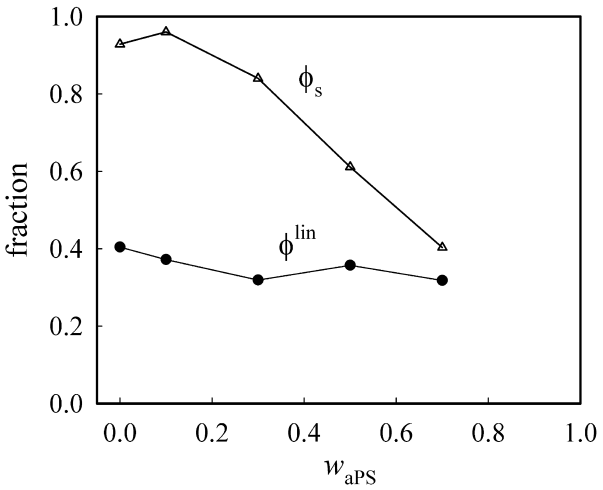


Fig. 12. Crystallinities of sPS/aPS blends as a function of aPS weight fraction.

of $\phi_v/\phi^{lin}$ is expected when some other domains besides the lamellar stacks have been developed in the bulk. From Fig. 12, the neat sPS and 90/10 blends are expected to be almost completely filled with lamellar stacks since the derived $\phi_s$ value is ca. 0.96. It is worthwhile to note that $\phi_s$ is larger than 0.5 if the weight fraction of aPS inclusion is less than 0.6. In other words, continuous sPS matrix is expected to form within blends with $w_{aPS} = 0.6$. For $w_{aPS} > 0.6$, dispersed sPS lamellar stacks are surrounded by non-crystallizable aPS matrix. This is consistent with thermo-mechanical properties of sPS/aPS blends reported by Bonnet et al. [34] who observed a plateau storage modulus up to a temperature as high as 250 °C for blends with $w_{aPS}$ up to 0.6.

It is instructive to compare the present results with iPS/aPS blends studied previously by Warner et al. [35] using a similar approach. Based on their SAXS results, both the long period and lamellar thickness of iPS remained unchanged on addition of aPS up to 30 wt%, leading to a constant $\phi^{lin}$. However, $\phi_v$ was found to decrease by an amount corresponding approximately to the dilution of iPS with aPS. For iPS/aPS blends, they concluded that segregation of the aPS to the interfibrilliar region of the spherulite occurs during iPS crystallization. Thus, in both sPS/aPS and iPS/aPS blend systems similar segregation morphologies have been confirmed.

### 3.2. TEM observation

To gain further insight into the morphology of sPS/aPS blends, electron microscopy was conducted and TEM images of $RuO_4$-stained blends are shown in Fig. 13 in which dark regions represent the selectively-stained amorphous phases and the bright lines refer to the crystalline lamellae. Those lamellae which are edge-on to the viewing direction can be readily observed. In addition to the presence of sPS lamellae, segregated domains of non-crystallizable aPS were found in between lamellar stacks, giving a typical interfibrillar segregation morphology. It suggests that majority of the added aPS component are rejected from the growing crystal front to a distance longer than that for the interlamellar segregation but shorter than that for the interspherulitic segregation. Th number and dimensions of the segregated aPS domains are increased with increasing aPS content. For 90/10 blends, the small dilution causes the difficulty in readily finding the segregated aPS domains. For 70/30 blends, the length and width of the segregated aPS domains are $315 \pm 55$ and $40 \pm 10$ nm, respectively. Segregated domains of $660 \pm 270$ nm long and $90 \pm 30$ nm wide are observed in the 50/50 blends. For 30/70 and 10/90 blends, however, the sPS lamellar stacks become dispersed in a matrix of non-crystallizable aPS. Large stacks consisting of dense lamellae parallel one another are well defined in the neat sPS and 90/10 blends. For blends with aPS content up to 50 wt%, stacks consisting of more than 5 lamellae are frequently observed, which supports the assumption and reliability of SAXS measurements required.

Using polarized optical microscopy to reveal the features with a length scale of μm, either spherulitic or axilitic structures can be observed in the neat sPS as well as in the sPS/aPS blends [36]. Both axilites and spherulites comprise regular packs of lamellar stacks. In fact, the axilites are under-developed sheaf-like features initiating from unidirectional growth of lamellar nuclei, which are distinguished from the general spherulites resulting from multidirectional growth of central nuclei. At the interior of spherulites (axilites), there exists a dense core of lamellar stacks. Near the spherulitic periphery, the splaying and fanning processes during lamellar growth result in appreciable spacing for lamellae to develop. In some locations, individual lamellae may even grow into the un-crystallized melt. Thus, it is important to recognize that the long periods at the periphery of a spherulite (or axilite) may be larger than those in the internal regions, where more compact lamellae are packed. As shown in the TEM image of 70/30 blends where impingement of three different lamellar stacks is evident, the inter-lamellar spacing is more open, giving a larger long period. Such observations accounts reasonably for the SAXS findings that both $L_c$ and $l_a$ are increased slightly with increasing aPS content until $w_{aPS} = 0.3$ (Fig. 11). No significant variation of $L_c$ and $l_a$ is found when more aPS is included in the blends. The interconnected sPS morphology is observed for blends with $w_{aPS} < 0.7$, indicative of dimensional persistence at high temperatures, which is consistent with SAXS results for $\phi_s$ (Fig. 12). As can be seen from TEM images, during the growth of sPS spherulites the melt aPS is incorporated in the interfibrillar regions by forming distinct domains within spherulites.

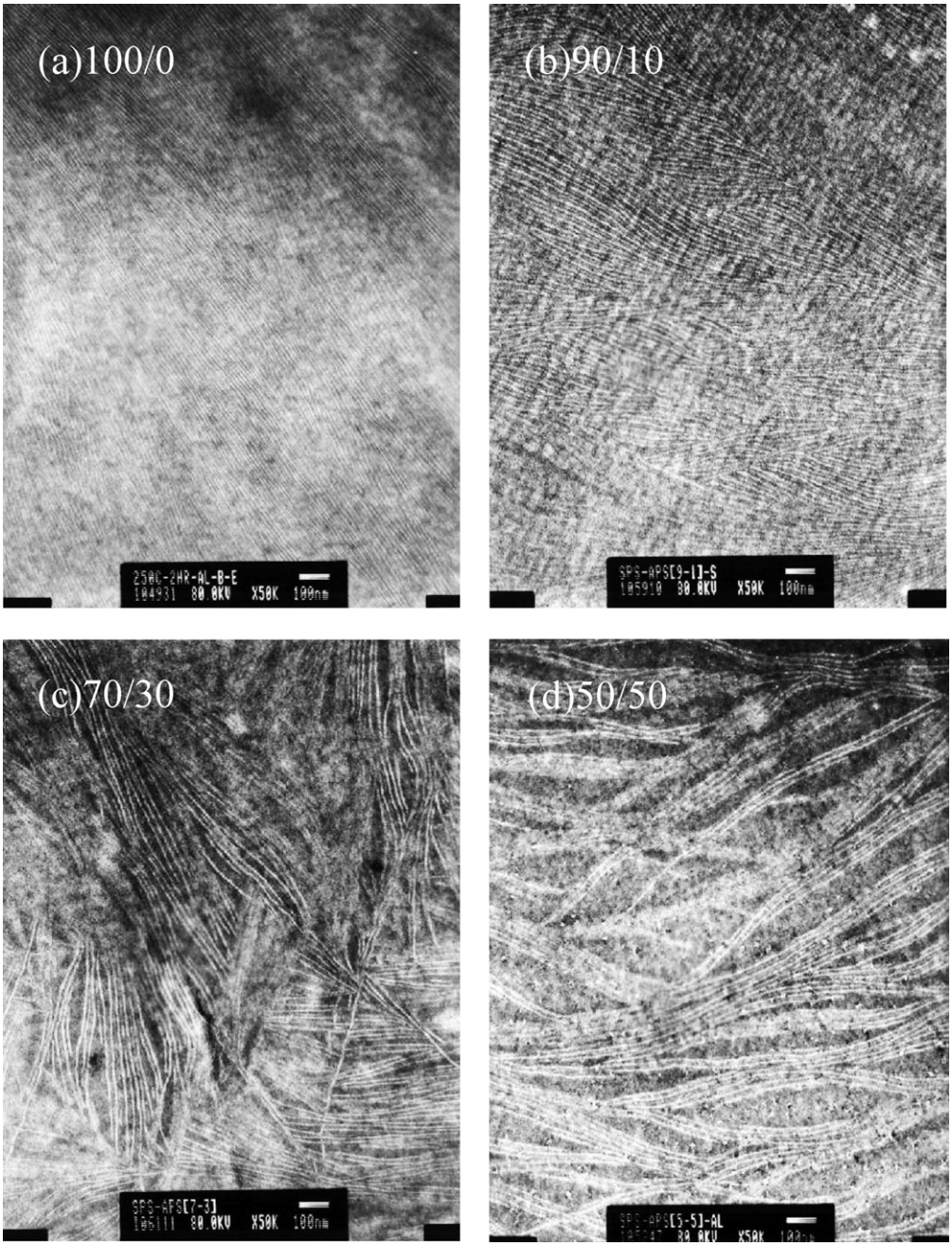


Fig. 13. TEM micrographs of sPS/aPS blends (a)100/0, (b) 90/10, (c) 70/30, (d) 50/50, (e) 30/70, and (f) 10/90.

## 4. Conclusions

sPS is a family of styrene polymer with superior solvent resistance and dimensional stability at high temperatures, compared with its counterparts, iPS and aPS. Effects of aPS content on the sPS lamellar thickness and aPS segregation were extensively investigated using SAXS and TEM. Because of the proximity of electron densities between the crystalline and amorphous phases, the SAXS reflection associated with lamellar morphology of sPS/aPS blends are weak at 25 °C, resulting in the difficulties in precise microstructure determination. High temperature SAXS is more appropriate to derive the accurate morphological parameters due to the enhanced contrast between the crystalline and amorphous phases. Based on the results obtained from the correlation approach, on addition of aPS, the amorphous layer thickness increases monotonically from 9.3 nm for neat sPS to 11.5 nm for 70/30 blends and then levels off up to 70 wt% aPS content, whereas the lamellar thickness decreases only slightly from 6.3 nm for neat sPS to 5.2 nm for 30/70 blends. The deduced long periods show a relatively maximum of 16.9 nm for 70/30 blends, compared to 15.6 and 16.3 nm for neat sPS and 30/70 blends, respectively. TEM images clearly show

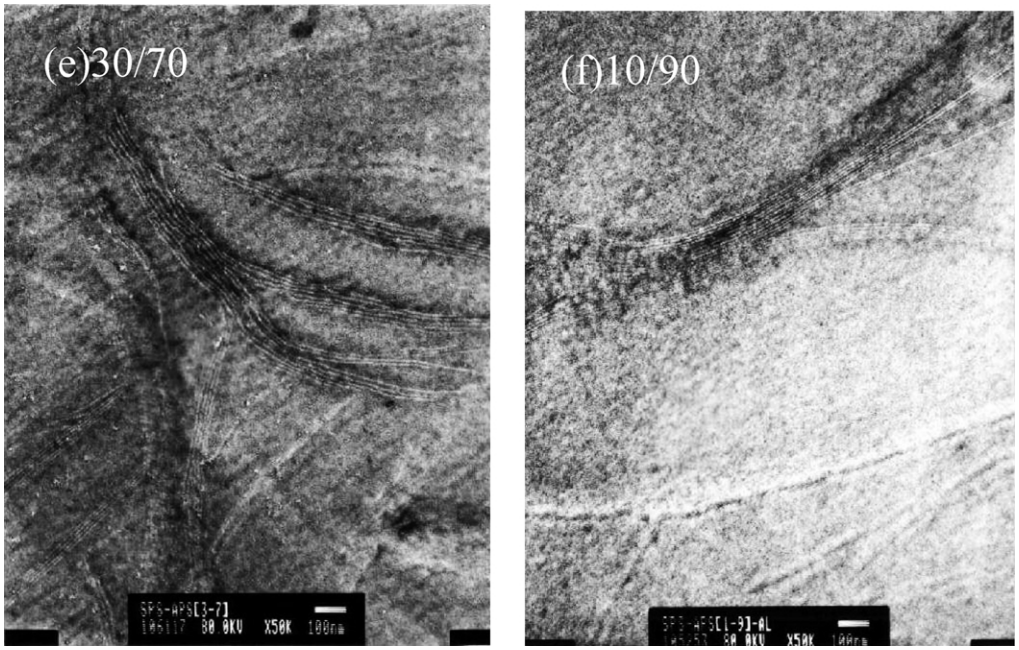


Fig. 13 (*continued*)

heterogeneity in the distribution of aPS volume within the spherulites. Judging from the TEM images of crystallized 70/30 blends, the increase of amorphous layer thickness is attributed to the more open lamellar stacks in the vicinity region of stack impingements, not resulting from the interlamellar segregation. It is evidently concluded from TEM observation that long periods at the periphery region of spherulites (or axilites) are larger than those in the central regions. Placement of the rejected aPS from the growth front occurs in the region between lamellar stacks, leading to an interfibrillar segregation.

## Acknowledgements

This work was supported by a grant from the National Science Council of the Republic of China (NSC91-2216-E-006-031).

## References

[1] Guerra G, Vitagliano VM, De Rosa C, Petraccone V, Corradian P. Macromolecules 1990;23:1539.
[2] Chatani Y, Shimane Y, Inoue Y, Inagaki T, Ijitsu T, Yukinari T. Polymer 1992;33:488.
[3] De Rosa C, Rapacciuolo M, Guerra G, Petraccone V, Corradini P. Polymer 1992;33:1423.
[4] Sun Z, Morgan RJ, Lewis DN. Polymer 1992;33:660.
[5] Tosaka M, Hamada N, Tsuji M, Kohjiya S, Ogawa T, Isoda S, Kobayashi T. Macromolecules 1997;30:4132.
[6] Cartier L, Okihara T, Lotz B. Macromolecules 1998;31:3303.
[7] Tosaka M, Tsuji M, Kohjiya S, Cartier L, Lotz B. Macromolecules 1999;32:4905.
[8] Wu H-D, Wu I-D, Chang F-C. Macromolecules 2000;33:8915.
[9] Ho RM, Lin CP, Tsai HY, Woo EM. Macromolecules 2000;33:6517.
[10] Woo EM, Lee ML, Sun YS. Polymer 2000;41:883.
[11] Bonnet M, Buhk M, Trogner G, Togausch KD, Petermann J. Acta Polym 1998;49:174.
[12] Hong BK, Jo WH, Kim J. Polymer 1998;39:3753.
[13] Woo EM, Wu FS. J Polym Sci, Polym Phys Ed 1998;36:2725.
[14] Chiu FC, Peng CG. Polymer 2002;43:4879.
[15] Park JY, Kwon MH, Park OO. J Polym Sci, Polym Phys Ed 2000;38:3001.
[16] Talibuddin S, Wu L, Runt J, Lin JS. Macromolecules 1996;29:7527.
[17] Hudson SD, Davis DD, Lovinger AJ. Macromolecules 1992;25:1759.
[18] Chen HL, Hsiao MS. Macromolecules 1998;31:6579.
[19] Liao WP, Lin TL, Woo EM, Wang C. J Polym Res 2002;9:91.
[20] Gianotti G, Valvassori A. Polymer 1990;31:473.
[21] Runt JP. Macromolecules 1981;14:420. The $\chi$ value of sPS/aPS blends was determined previously to be $-0.04$ to $-0.11$ in Ref. [10] using the Flory–Huggins equation. The discrepancy between theirs and ours is attributed to the molecular weight distribution of aPS used. Although high MW aPS ($M_w = 192$ kg/mol) was also applied in Ref. [10], the polydispersity was too large ($\sim 5.1$) which resulted in a broad transition breadth of glass transition (11.5 °C) and a rather low $T_g$ (85.6 °C). It leads to the necessity to consider the entropic contribution in deriving appropriate interaction parameter from the Flory–Huggins theory.
[22] Flory PJ. Principles of polymer chemistry. Ithaca, NY: Cornell University Press; 1953. Nishi T, Wang TT. Macromolecules 1975;8:909.
[23] Wang C, Hsu YC, Lo CF. Polymer 2001;42:8447.
[24] Wang C, Cheng YW, Hsu YC, Lin TL. J Polym Sci, Polym Phys Ed 2002;40:1626.
[25] Nojima S, Terashima Y, Ashida T. Polymer 1986;27:1007.
[26] Schultz JM. J Polym Sci, Polym Phys 1976;14:2291.
[27] Miyamoto Y, Fukao K, Miyaji H. Colloid Polym Sci 1995;273:66.
[28] Statton WO. J Polym Sci 1956;22:385.
[29] Barnes JD, Mckenna GB, Landes BG, Bubeck RA, Bank D. Polym Engng Sci 1997;37:1480.
[30] Strobal GR, Schneider M. J Polym Sci, Polym Phys Ed 1980;18:1343.
[31] Andjelić S, Jamiolkowski D, Mcdivitt J, Fischer J, Zhou J, Wang ZG, Hsiao BS. J Polym Sci, Polym Phys Ed 2001;39:153.

[32] Baltá-Calleja FJ, Vonk CG. X-ray scattering of synthetic polymers. New York: Elsevier; 1989. p. 247.
[33] Bark M, Zachmann HG. Makromol Chem 1992;193:2363.
[34] Bonnet M, Buhk M, Petermann J. Polym Bull 1999;42:353.
[35] Warner FP, MacKnight WJ, Stein RS. J Polym Sci, Polym Phys Ed 1977;15:2113.
[36] Wang C, Chen CC, Cheng YW, Liao WP, Wang ML. Polymer 2002; 43:5271.